Excitation of Surface Plasmons Using Tilted Planar-Waveguide Bragg Gratings
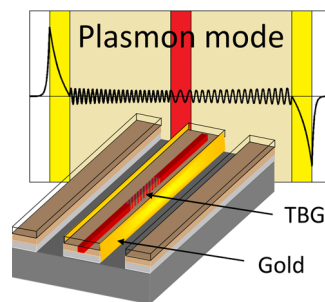
C. Holmes
K. R. Daly
I. J. G. Sparrow
J. C. Gates
G. D'Alessandro
P. G. R. Smith

Excitation of Surface Plasmons Using Tilted Planar-Waveguide Bragg Gratings

C. Holmes,[1*] **K. R. Daly,**[2] **I. J. G. Sparrow,**[3] **J. C. Gates,**[1] **G. D'Alessandro,**[2] **and P. G. R. Smith**[1]

[1]Optoelectronics Research Centre, University of Southampton, SO17 1BJ, Southampton, U.K.
[2]School of Mathematics, University of Southampton, SO17 1BJ, Southampton, U.K.
[3]Stratophase Ltd., SO51 9DL, Romsey, U.K.

Abstract: We present a planar-integrated optical surface plasmon refractometer. The fabricated device operates by grating-matched coupling between a core waveguide mode and a set of hybrid plasmon-dielectric modes of a much wider integrated structure. The constructed device incorporates a 50-nm-thin gold layer that separates a tilted planar-waveguide Bragg grating and a liquid analyte. It is demonstrated that polarization-dependent plasmon anomalies occur in the transmission spectra of the device, which are understood using a numerical Cauchy integral mode solving approach. Sensitivities in this planar-integrated device are comparable with existing fiber-based plasmonic sensors but with the advantages of planar integration and microfluidic adaptation.

Index Terms: Waveguides, plasmonics, gratings, sensors.

1. Introduction

The motivation to develop waveguide Surface Plasmon Resonance (SPR) sensors is strong, as moving from a bulk optics regime [1], [2] to an optical waveguide regime offers a number of important advantages in real applications in terms of ruggedness, stability, and small form factor. The steps to realize such devices have been the subject of many theoretical and experimental investigations [2]–[5]. The first reported demonstration of an optical waveguide being used to excite an SPR was made by Jorgensen and Yee [3]. In this paper, a multimode optical fiber had its cladding stripped and replaced with a thin metal layer. The device essentially operated in a Kretschman configuration [2] which is the means of operation for many current commercial waveguide-SPR sensors. Recently, this concept has been expanded by engineering Tilted Bragg Grating (TBG) structures within an optical waveguide to efficiently couple light into plasmon excitations. TBG-SPR devices overcome the wave vector mismatch between a guided core mode and a plasmon mode (in a thin metallic layer) by using the phase-matching properties of the grating. These devices efficiently couple light into plasmon modes, have an inherent temperature referencing capability [6] and can utilize existing Bragg grating interrogation systems for characterization. The work reported in this paper expands TBG-SPR operation still further by integrating it into an optical planar waveguide regime. Whereas previously TBG-SPR structures have been confined to optical fiber waveguides [5]–[10], this new concept offers the added advantages of planar integration. While metal-coated fibers may be appropriate for some applications, their small size and cylindrical format make sealing them into microfluidics complicated, and they do not naturally lend themselves to creating densely packed sensor arrays for multiple
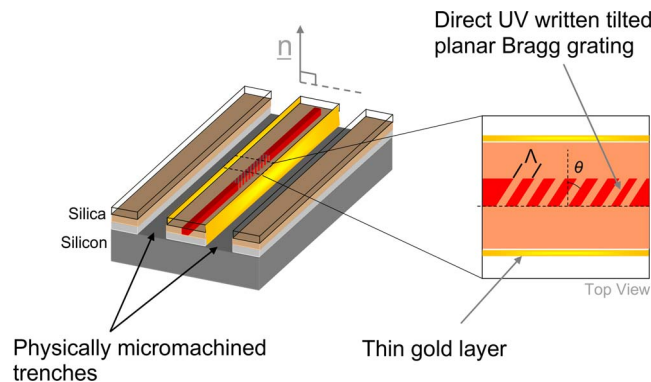
Fig. 1. Schematic of a tilted planar Bragg grating surface plasmon resonance sensor (n.b.—gold deposited over the whole sample, but only side walls are shown for illustration).

targets. Planar integration can overcome these challenges by offering the ability to detect multiple biohazard threats on a single chip [11]. Such a planar geometry also lends itself to the creation of more complex hybrid metallic grating structures such as those proposed by Tripathi *et al.* [12].

From a fabrication perspective, the planar-integrated format simplifies the deposition of a uniform gold layer and inherently maintains the polarization of the input optical field, which is an important feature for TBG-SPR devices [9]–[10]. In this paper, the fabrication is implemented via a recently reported rapid prototyping technique that combines Direct UV Writing (DUW) and physical micromachining to achieve a planar TBG waveguide [13]. Fig. 1 illustrates the presented device that consists of a single-mode waveguide containing the TBG created by DUW and two physically machined channels running parallel to the core located either side of it. This approach to fabrication is fully computer controlled, allowing design flexibility of any 2-D waveguide structure, grating tilt angle, and lateral cladding width. In addition, as the physically machined trenches are of micrometer size, they form a delivery system that can exploit microfluidic operation. The fabricated device has a blazed grating angle of 10° and a ridge width of 125 μm, such that the presented results can be compared with previously reported TBG-SPR devices in optical fibers [5]–[10].

A theoretical understanding of experimental data is made through numerically finding the waveguide and plasmonic modes using a Cauchy integral method [14] and known dispersion relations. Corresponding spectral features are subsequently inferred using the phase matching condition, as detailed in the following section.

2. Theory and concept

A TBG scatters light into different waveguide modes. As a condition of orthoganality, the grating planes must be tilted in order to promote efficient coupling. A forward propagating core mode of effective index n_{eff} can be coupled into an ith contra-propagating cladding mode of effective index n^i_{clad} through purposely blazing grating planes, following the phase matching condition

$$\lambda^i_{clad} = \frac{(n_{eff} + n^i_{clad})\Lambda}{\cos\theta} \qquad (1)$$

where a grating of pitch Λ has planes tilted relative to the axes of the waveguide by an angle θ, as illustrated in Fig. 1. Coupling results in a spectral feature located at wavelength λ^i_{clad}. For the situation in which a thin metal layer is deposited on the device an additional set of modes, pure and hybrid plasmonic modes [4] can also be excited. Typically, this occurs when the magnetic field is in the plane of the metal layer. As the metal layer, in the constructed device, is perpendicular to the planar layer, the respective pure plasmon mode is categorized as a Transverse Electric (TE) mode relative to the overall structure. It should be noted that strictly plasmon modes are designated as being Transverse Magnetic (TM) polarizations [4]; however, in this case, our choice of TE designation is just a matter of
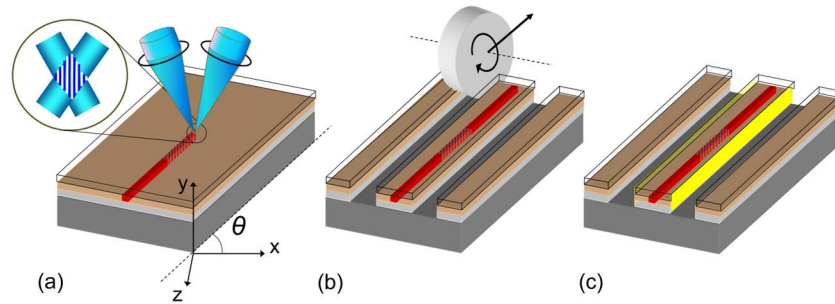
Fig. 2. Three-stage technique used to fabricate the planar TBG-SPR device depicting (a) direct UV writing, (b) physical micromachining, and (c) sputtering of a thin gold layer.

description as through convention, we choose the plane of the chip to be the transverse direction, and not the plane layer of the gold. To avoid confusion, Fig. 1 contains the vector n, indicating the magnetic field direction in the core waveguide that excites the plasmon in the gold.

Mode solutions were theoretically calculated using the aforementioned Cauchy integral method and the effective index method. The solutions provide effective indices of all supported modes: both leaky and bound. Spectral features were inferred through combining these solutions with the phase matching condition [see (1)]. The parameters assumed in the numerical model are detailed in the following section alongside a description of device fabrication.

3. Fabrication

Device fabrication began by growing a thick (16.5 μm) thermal oxide layer upon a silicon wafer and consolidating two silica layers upon one side using Flame Hydrolysis Deposition (FHD). The core silica layer was doped with germanium and boron to make it photosensitive to UV light. Photosensitivity was further enhanced through hydrogen loading the sample for 1 week at 12 MPa. A single-mode waveguide and TBG were defined into the core layer using a dual beam DUW technique [11], [15], which is illustrated in Fig. 2(a). The fabricated device had a compensated grating pitch $\Lambda/\cos(\theta)$ of 540.4 nm, a grating length of 5 mm, and was designed to guide an optical mode, matched to SMF-28. After DUW, two trenches were diced on either side of the UV written TBG, with a nickel-bonded diamond blade, to define a 125-μm lateral cladding dimension, which is illustrated in Fig. 2(b). The remaining hydrogen was then removed through an annealing step (200 °C for 5 days). Light was launched into the planar waveguide using fiber pigtails that were secured to the chip using UV curing epoxy. The final fabrication step involved the sputtering of a thin (50-nm) gold layer onto the device, which is illustrated in Fig. 2(c). Sputtering ensured relatively uniform deposition coverage, compared with alternative techniques such as e-beam or thermal evaporation. Gold thickness can be controlled on the vertical walls of the trenches by calibrating the sputtering chamber used.

Using a Metricon prism coupler, the underclad (thermal oxide), core, and overclad layers had been determined to have refractive indices of 1.444, 1.4539, and 1.4447 at 1550 nm wavelength, respectively. The thickness of the core layer was 6.2 μm, and the cladding layers had thicknesses >15 μm. The lateral width of the ridge formed between the two physically micromachined trenches was measured with a light microscope to be 125 $\pm$ 1 μm. Numerical simulation used these measurements as initial values and applied a fitting algorithm, which incorporated the effective index method, to fit modal solutions to measured spectral features, prior to a gold deposition. The assumed vertical effective refractive index of the core waveguide and cladding were 1.4530 and 1.4474, respectively, at 1550 nm and single mode. Due to the thickness of the underclad, the mode did not penetrate the silicon. Likewise, due to the thickness of the overclad, the mode did not penetrate the gold deposited upon the top of the waveguide. The DUW waveguide was assumed to have a lateral width of 7.0 μm and the gold a lateral width of 50 nm. Using calibrated Sellmeier equations for the written waveguide [16] and Cauchy equations for refractive index fluids (used to calibrate device sensitivity), the dispersion of the system was included in the model.
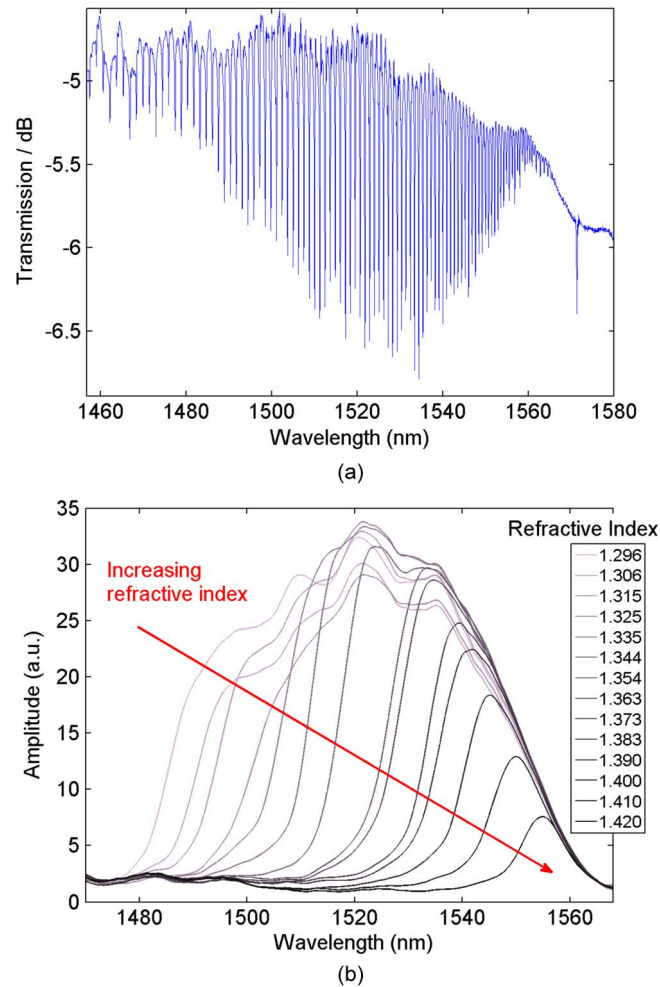
Fig. 3. (a) TE transmission spectrum of a 10° planar tilted Bragg grating and (b) a representation of the cladding mode envelope subject to analytes of different refractive indices.

4. Measurements

To characterize the grating spectra, a tunable laser was spectrally scanned and the transmitted power measured. This was made for the same device prior to gold deposition (native device) and subsequent to gold deposition. For both conditions, sensitivity curves were obtained using Cargille refractive index fluids ranging from indices of 1.296 to 1.430 at 1550 nm (series AAA and AA).

4.1. Native Device

The transmission spectrum for the native device is shown in Fig. 3(a); it contains a guided core mode and an envelope of cladding modes. In order to interpret the cladding mode envelope, a moving standard deviation method was applied [13], using a window width of 1.25 nm. This technique infers the envelope amplitude by calculating the standard deviation, in transmitted power, for a finite spectral bin scanned over the complete wavelength range. Fig. 3(b) illustrates the evolution of envelope amplitude with increasing external refractive index fluid. It can be observed that as the external refractive index increases guided modes reach cutoff $n_{oil} > n_{clad}^{i}$ and become leaky. This phenomenon is observed for both orthogonal states of linear polarization.

A thorough understanding of the mode structure of this device can be obtained from numerical simulation. Using the Cauchy integral method, the modes supported by the waveguide can be found.
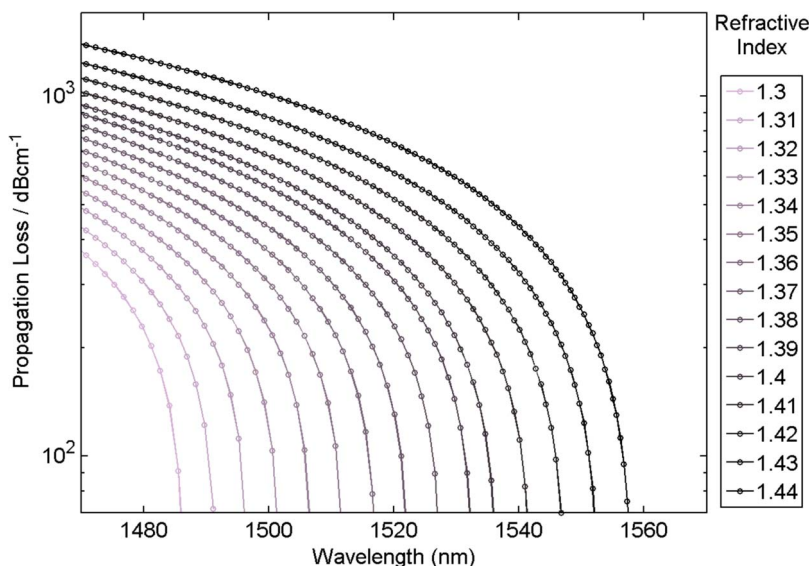
Fig. 4. Numerical solutions for TE cladding modes and their dependence upon the refractive index of the measured analyte.

Fig. 4 illustrates the discrete set of leaky mode solutions for the system. In this illustration, the dispersive part of the mode solutions have been converted to wavelength [using (1)] and the extinction coefficient converted to propagation loss. A marker indicates the discrete solution, and a line connecting the markers is present to aid interpretation. It can be seen that the leaky mode solutions have an associated high attenuation value (of the order 10^3 dB/cm). This large attenuation corresponds to the absence of spectral features associated with cutoff that is observed experimentally. As with experimental data, both orthogonal polarizations display a comparable response.

To interpret cutoff from experimental data, a maximum derivative technique was used [7]. Fig. 5(a) tracks cutoff as a function of refractive index unit (riu), showing a response of 541.9 nm/riu for TE and 536.8 nm/riu for TM polarizations. These were calculated using a linear least square fit algorithm, the standard deviation in vertical offset being 1.9 nm for TE and 1.2 nm for TM polarizations. Cutoff can be tracked through numerical simulation by monitoring the guided-leaky mode boundary. Fig. 5(b) tracks the theoretical cutoff as a function of refractive index, calculated by monitoring modes with a propagation loss greater than 2 dB over 5 mm (4 dB/cm). This value was chosen as the spectral features of the cladding modes observed in Fig. 3(a) are of the order 2 dB, and the length of the Bragg grating is 5 mm. For TE polarization, the sensitivity was 500.7 nm/riu and for the TM polarization was 500.9 nm/riu. The vertical offset standard deviations, for these least square fits, were 0.4 nm for both polarizations.

4.2. Plasmon Anomalies

The envelope profiles of the same device, after a 50-nm deposition of gold are illustrated in Fig. 6(a) and (b) for TM and TE polarizations, respectively. Both orthogonal states of linear polarization show different spectral responses, both to each other and to the native case.

For TM polarization, the presence of different refractive index fluids has a negligible effect on the cladding mode envelope. It is understood from electromagnetic theory that as the waveguide and analyte have permeabilities equal to unity, a surface plasmon mode cannot be supported for this polarization [4]. Hence, the evanescent field of the mode does not penetrate into the trenches and is not affected by changes of the refractive index oil.

For TE polarizations, the transmission spectrum is affected by the presence of different refractive index fluids, as illustrated in Fig. 6(b). However (unlike the native case), there is no significant cutoff
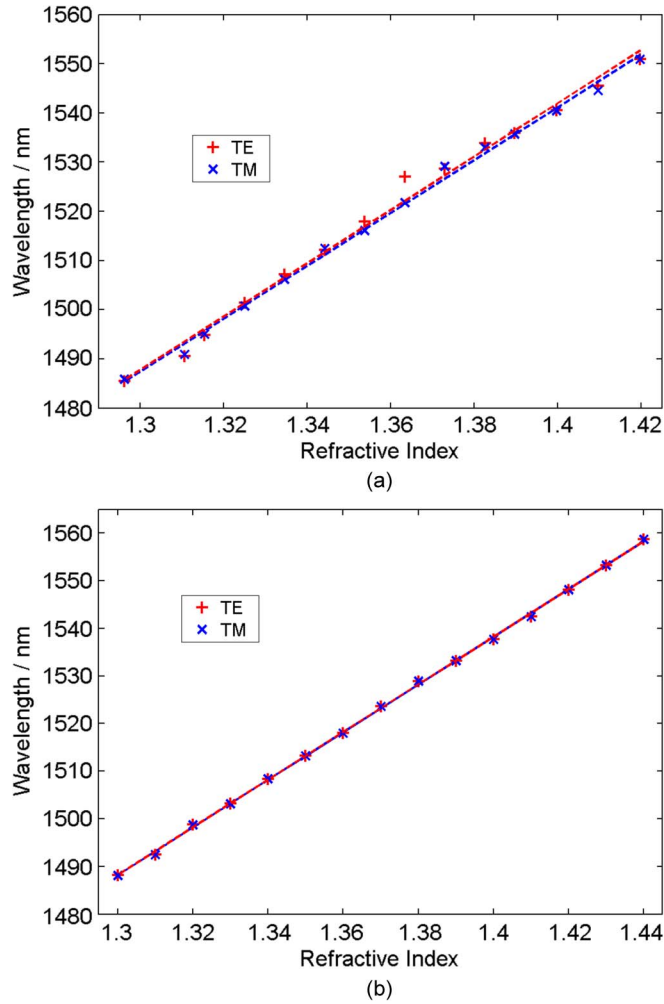
Fig. 5. (a) Tracking the point of maximum positive gradient for the experimental cladding mode envelope data. (b) The theoretical cutoff location for the device as a function of refractive index.

effect. There is, however, an additional effect for refractive indices between 1.296 (n.b. the lowest available refractive index liquid in the Cargille series) and 1.420, essentially appearing as an anomalous region of high loss that shifts to larger wavelengths as refractive index fluid is increased. This effect is understood to be the result of a plasmon anomaly and has been reported in TBG-SPR devices in optical fiber [5]–[10].

A pure surface plasmon typically exists at the interface between a semi-infinite metal and a dielectric layer. The mode supported has its magnetic field transverse to the plane of the gold layer. As the gold layer in this instance is perpendicular to the transverse core layer, this is labeled a TE mode. The effective index of such a mode is [1]

$$n_{spp} = \sqrt{\frac{n_d^2 n_m^2}{n_d^2 + n_m^2}} \qquad (2)$$

where n_d is the refractive index of the dielectric, and n_m is the refractive index of the metal. The waveguide studied here supports two families of these modes, the effective indices of which can be approximated by (2). This is to say approximated as a pure surface plasmon, existing between two semi-infinite layers. The first family of modes is associated with the interface between the gold layer and the silica (in other words the inner gold interface). In typical operation, when the silica index is
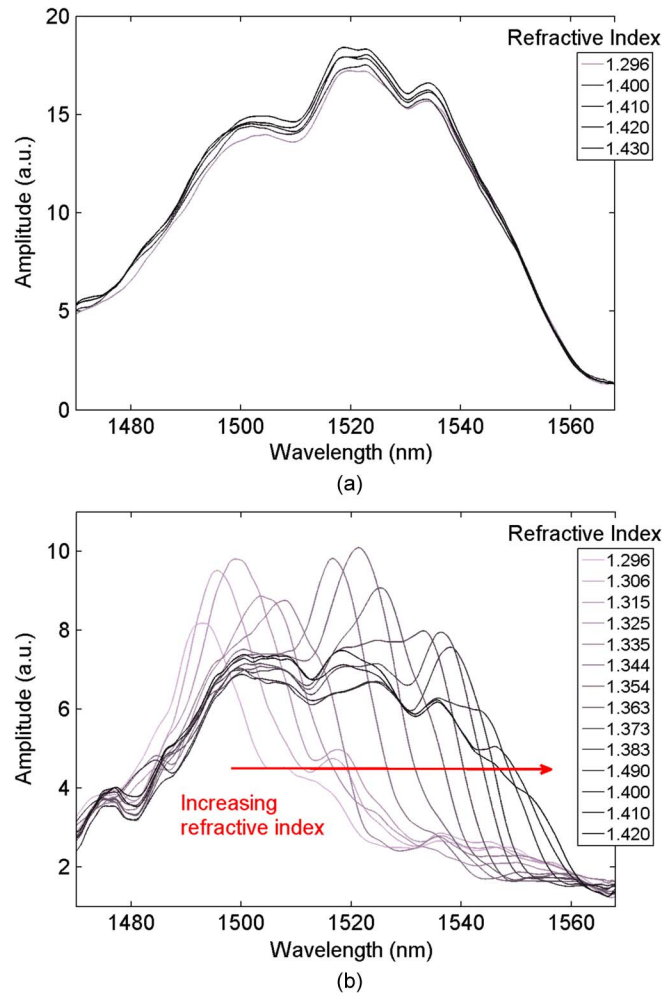
Fig. 6. Amplitude envelope of cladding mode resonances, for (a) TM and (b) TE polarizations, with a gold deposit.

greater than that of the analyte, the effective index of these modes is larger than any other mode. The modes are localized, one at each silica-gold interface and due to their strong attenuation in the gold layer, they are insensitive to changes in the index oil and therefore play no role in sensing. The second family of modes exists at the interface between the gold and the analyte (in other words the outer gold interface). These modes typically have effective indices lower than the silica. Therefore, they are less localized and can interact with plasmon modes on the far side of the device. These modes are highly sensitive to changes in the index oil, as shown by (2), and correspond to the region of high loss observed in the TE orientation.

A more thorough understanding of this system can be obtained from numerical simulation. The mode solutions can explain the experimental phenomena of negligible cutoff for both TE and TM polarization and the region of high loss observed in the TE orientation.

Numerical solutions for the TM polarization are illustrated in Fig. 7(a). These values are insensitive to changes in refractive index, as are those observed experimentally [see Fig. 6(a)]. The negligible cutoff effect observed experimentally can also be explained using numerical simulation. Comparing Fig. 4 with Fig. 6(a), it is apparent that the modal solutions for the gold case have a relatively small propagation loss: on the order 1 dB/cm compared with 10^3 dB/cm for the native device. As this attenuation is small, the spectral features corresponding to modal solutions can still be observed experimentally. Effectively, the gold acts to screen the mode from the analyte, thereby retaining the optical power within the cladding
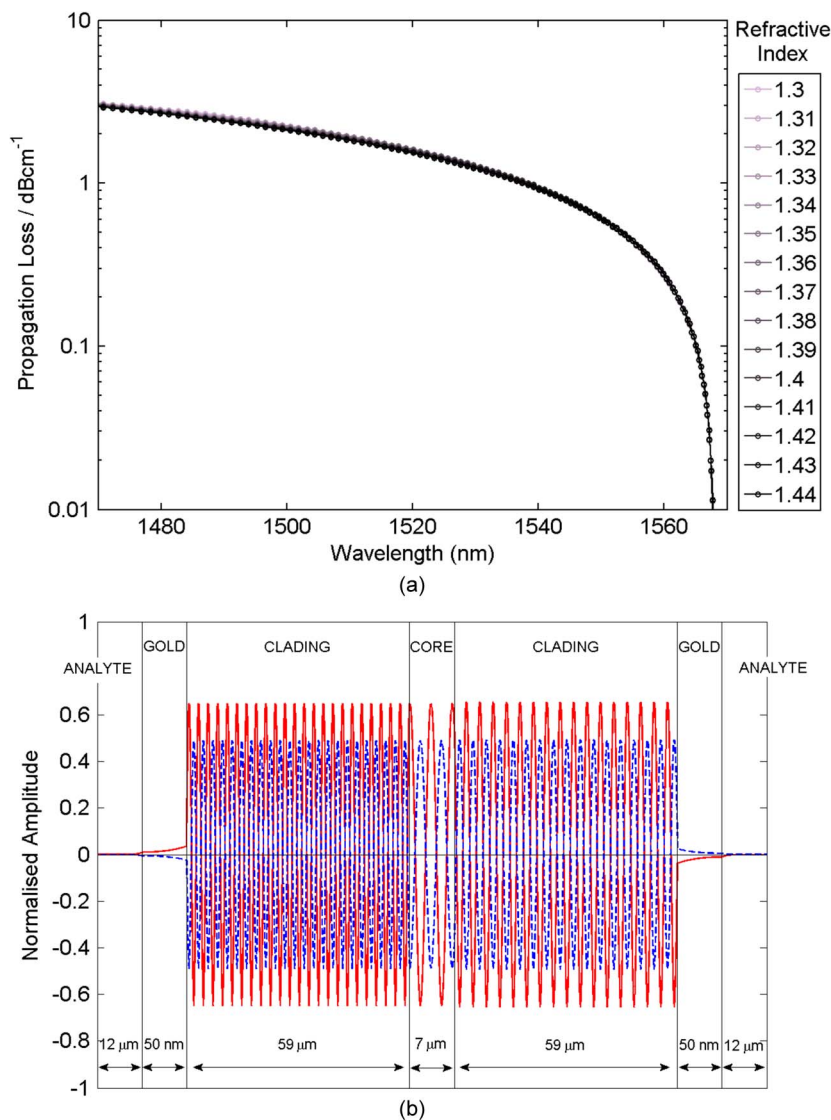
Fig. 7. (a) TM numerical mode solutions for the gold coated device and (b) the electric mode field amplitude for the spectral feature at 1520 nm (red line corresponding to real part, dashed blue line corresponding to imaginary part), for an analyte of refractive index 1.44 (n.b.—the layer thicknesses are not relatively scaled).

region. Fig. 7(b) illustrates this through an amplitude profile of the mode. The represented mode corresponds to a 1520-nm spectral feature, with an analyte refractive index of 1.44. The dimensions of the respective horizontal layers have been scaled such that features can be resolved.

Numerical mode solutions for the TE polarization are illustrated in Fig. 8(a). The form of these solutions is distinctly different to those of the native device, illustrated in Fig. 4. First, there is no cutoff effect resulting from large propagation loss of supported modes. The propagation loss is generally small (of the order 1 dB/cm), and thus, the shape of the envelope is conserved for certain refractive indices. In addition, there is a high loss peak, corresponding to the plasmon modes whose power is concentrated at the analyte-gold interface. There is, in fact, a family of modes about this peak that have some pure plasmon and some guided mode characteristics. Fig. 8(b) illustrates the amplitude profile of the highest loss plasmon mode, for an analyte refractive index of 1.44. This mode most closely approximates that of a pure plasmon at the analyte-gold interface, which is given by (2). This
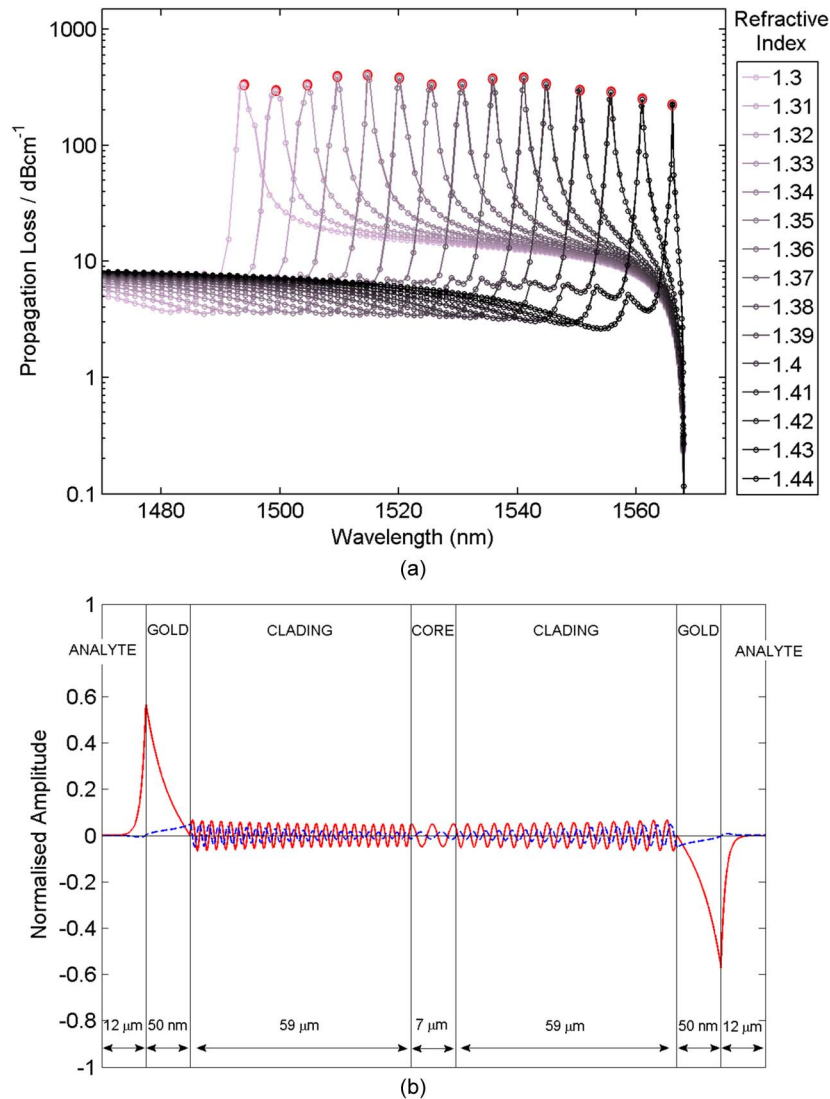
Fig. 8. (a) TE numerical mode solutions for the gold coated device. The highest loss mode, corresponding to a hybrid plasmon mode, is highlighted by a red circle and (b) the magnetic mode field amplitude for the high loss plasmon mode (red line corresponding to real part, dashed blue line corresponding to imaginary part), for an analyte of refractive index 1.44 (n.b.—the layer thicknesses are not relatively scaled).

high loss peak (of the order 10^3 dB/cm) corresponds to the lossy region observed experimentally, which shifts with respect to variations in the analyte's refractive index.

It must be noted that experimentally for an analyte refractive index of 1.0, the shape of the cladding mode envelope is comparable with that at an index of 1.420, albeit with a lower overall amplitude ($\sim$1.36 dB). This can be understood through numerical simulation. At an analyte refractive index of 1.0, the plasmon mode is at a wavelength much shorter than the cladding mode envelope. For an analyte refractive index of 1.420 and above, the plasmon mode is at wavelengths much longer than the cladding mode envelope. Thus, at these extremes, the plasmon mode does not affect the form of the cladding mode envelope. For an analyte refractive index of 1.0, the experimental measurement has a lower overall amplitude (compared with 1.420) because the propagation losses for wavelengths longer than the plasmon mode are greater than for those of shorter wavelength, which is a trend that is evident in Fig. 8(a).
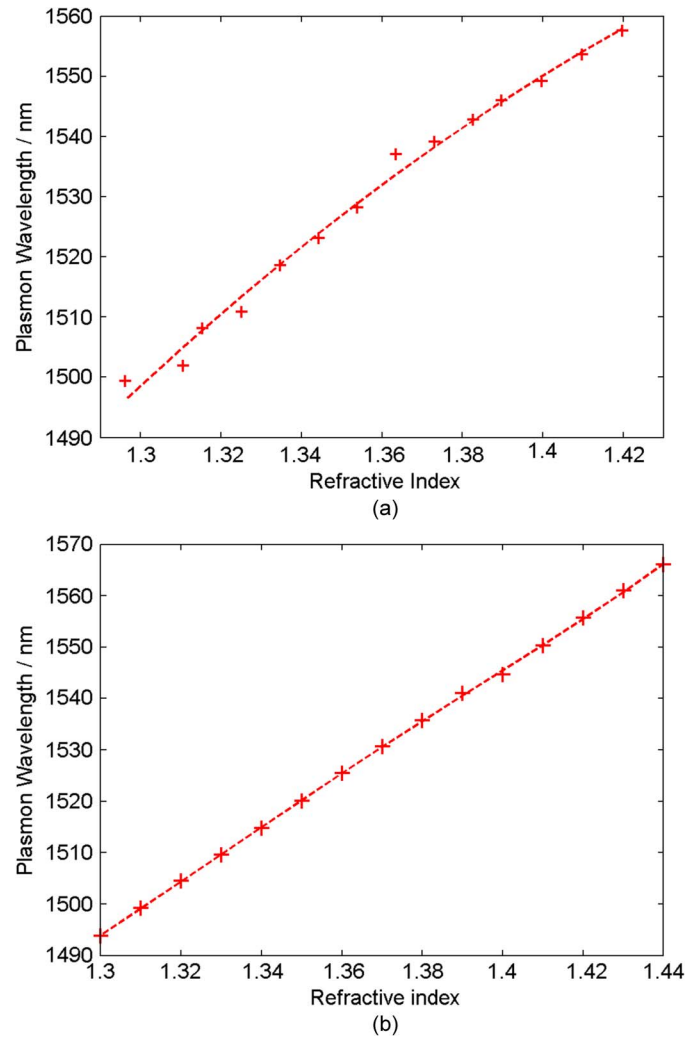
Fig. 9. (a) Tracking the point of maximum negative gradient (TE plasmon anomaly) as a function of refractive index oil for the measured TE polarization. (b) Tracking the spectral positioning of the plasmon mode with respect to variations measurand refractive index.

The sensitivity of the plasmon anomalies in the experimental data can be inferred through tracking the largest negative gradient of the envelope [7], which is illustrated in Fig. 9(a). The sensitivity of this curve is 566.9 nm/riu, and the fit had a standard deviation of 1.5 nm. This is comparable with similar constructed devices in optical fiber that quote 571.5 nm/riu [6]. The simulated plasmon shift was obtained through tracking the peak propagation loss, which is illustrated in Fig. 9(b). The maximum sensitivity of the mode was 531.2 nm/riu (at n = 1.327), which is a value comparable with that shown experimentally. The standard deviation of this fit is 0.2 nm.

5. Discussion

Using a maximum gradient technique [7], the bulk refractive index resolution for a native device is 2.2×10^{-3} riu, compared with 2.6×10^{-3} riu for a gold enhanced device. Despite the slightly lower optical sensitivity with the enhancement layer, it must be noted that a pure plasmon mode concentrates optical power in a very small localized area at the gold-analyte interface. Combined with the catalog of surface functionalization chemistry that can be exploited using gold [2], the potential for surface-sensitivity enhancement is increased. In addition, as the TM polarization is insensitive to the analyte, it can be used for temperature referencing.

In this paper, the device was fabricated to match parameters of previously reported TBG-SPR designs in optical fiber, and the sensitivities of these respective regimes were comparable. Future devices will look to improve performance by tailoring device dimensions and adopting strategies of individual resonance tracking [8]. The design flexibility associated with physical micromachining permits any lateral cladding dimension to be easily fabricated. Altering dimension size can either reduce (for smaller widths) or increase (for larger widths) the density of resonance features. This is important when tracking individual modes as more features enhance resolution; however, if the mode density is too great, individual features can be misinterpreted for others. The flexibility of this technique gives complete control on this parameter, which can be manipulated, depending upon desired operation. The manipulation of cladding thickness for SPR-TBG devices has been reported in fiber geometry [17], but this typically requires either hazardous etchants such as HF or complex and time-consuming fabrication processes such as lapping and polishing.

Through using a Cauchy integral method, the spectral plasmon phenomena measured experimentally has been theoretically understood. Both theoretical and experimental sensitivities are comparable, suggesting that the method of simulation can be used to further tailor device operation.

6. Conclusion

The first demonstration of a planar SPR-TBG refractometer has been reported. The novel device has been fabricated by combining direct UV and physical micromachining techniques. These processes permit greater design flexibility and usability. In addition, this is the first time experimental observation of such a device has been rigorously correlated with modeling, and thereby, the origin of the spectral features are fully understood.

The spectral response of the reported device had anomalous plasmon effects, including a distinctly different response between orthogonal polarizations, no spectrally observed cutoff, and a plasmon-associated high loss region that was dependent upon the refractive index of the analyte. Using a numerical mode solving technique, which solved leaky and bound modes, these anomalies were theoretically explained.

Tracking spectral sensitivity of a plasmon mode experimentally, using a maximum negative gradient method, concluded a maximum spectral shift of 566.9 nm/riu. This value is of a comparable order to the shift theoretically predicted through simulation and values obtained in similar formats using optical fiber geometry.

The development of this technology from optical fiber to a planar platform permits denser integration, miniaturization, and microfluidic possibilities. The specific fabrication processes of DUW and physical micromachining increases design flexibility through allowing cost-effective rapid prototyping solutions.

References

[1] H. Raether, *Surface Plasmons*. New York: Springer-Verlag, 1988.

[2] I. Abdulhalim, M. Zourob, and A. Lakhtakia, "Surface plasmon resonance for biosensing: A mini-review," *Electromagnetics*, vol. 28, no. 3, pp. 214–242, Sep. 2008.

[3] R. C. Jorgenson and S. S. Yee, "A fibre-optic chemical sensor based on surface plasmon resonance," *Sens. Actuators B, Chem.*, vol. 12, no. 3, pp. 213–220, Apr. 1993.

[4] R. Kashyap and G. Nemova, "Surface plasmon resonance-based fiber and planar waveguide sensors," *J. Sensors*, vol. 2009, pp. 645 162-1–645 162-9, Jun. 2009.

[5] Y. Y. Shevchenko and J. Albert, "Plasmon resonances in gold-coated tilted fiber Bragg gratings," *Opt. Lett.*, vol. 32, no. 3, pp. 211–213, Feb. 2007.

[6] L.-Y. Shao, Y. Shevchenko, and J. Albert, "Intrinsic temperature sensitivity of tilted fiber Bragg grating based surface plasmon resonance sensors," *Opt. Exp.*, vol. 18, no. 11, pp. 11 464–11 471, May 2010.

[7] Y. Lu, R. Geng, C. Wang, F. Zhang, C. Liu, T. Ning, and S. Jian, "Polarisation effects in tilted fiber Bragg grating refractometers," *J. Lightw. Technol.*, vol. 28, no. 11, pp. 1677–1683, Jun. 2010.

[8] B. Špaèková, M. Piliarik, P. Kvasnièka, C. Temistos, M. Rajarajan, and J. Homola, "Novel concept of multi-channel fiber optic surface plasmon resonance sensor," *Sens. Actuators B, Chem.*, vol. 139, no. 1, pp. 199–203, May 2009.

[9] Y. Shevchenko, C. Chen, M. A. Dakka, and J. Albert, "Polarisation-selective grating excitation of plasmons in cylindrical optical fibres," *Opt. Lett.*, vol. 35, no. 5, pp. 637–339, Mar. 2010.

[10] C. Caucheteur, Y. Shevchenko, L.-Y. Shao, M. Wuilpart, and J. Albert, "High resolution interrogation of tilted fiber grating SPR sensors from polarization properties measurement," *Opt. Exp.*, vol. 19, no. 2, pp. 1656–1664, Jan. 2011.

[11] D. Bhatta, A. Michel, M. Marti Villalba, G. D. Emmerson, I. J. G. Sparrow, M. B. McDonnell, E. A. Perkins, R. W. Ely, and G. A. Cartwright, "Optical Microchip Sensors for Multiplexed Detection of Biological Pathogens," Eur. Lab. Autom.; Hamburg, Germany, Jun. 30–Jul. 1, 2011.

[12] S. M. Tripathi, A. Kumar, E. Marin, and J. Meunier, "Highly sensitive miniaturized refractive index sensor based on Au-Ag surface gratings on a planar optical waveguide," *J. Lightw. Technol.*, vol. 28, no. 17, pp. 2469–2476, Sep. 2010.

[13] C. Holmes, L. G. Carpenter, H. L. Rogers, I. J. G. Sparrow, J. C. Gates, and P. G. R. Smith, "Planar waveguide tilted Bragg grating refractometer fabricated through physical micromachining and direct UV writing," *Opt. Exp.*, vol. 19, no. 13, pp. 12 462–12 468, Jun. 2011.

[14] E. Anemogiannis and E. N. Glytsis, "Multilayer waveguides: efficient numerical analysis of general structures," *J. Lightw. Technol.*, vol. 10, no. 10, pp. 1344–1351, Oct. 1992.

[15] G. D. Emmerson, S. P. Watts, C. B. E. Gawith, V. Albanis, M. Ibsen, R. B. Williams, and P. G. R. Smith, "Fabrication of directly UV-written channel waveguides with simultaneously defined integral Bragg gratings," *Electron. Lett.*, vol. 38, no. 24, pp. 1531–1532, Nov. 2002.

[16] H. L. Rogers, C. Holmes, J. C. Gates, and P. G. R. Smith, "Direct refractive index measurement technique to observe waveguide dispersion characteristics of short waveguides utilizing the higher order modes of integrated Bragg grating structures," in *Proc. CLEO Europe-EQEC*, Munich, Germany, May 22–26, 2011, p. 1.

[17] T. Allsop, R. Neal, S. Rehman, D. J. Webb, D. Mapps, and I. Bennion, "Generation of infrared surface plasmon resonances with high refractive index sensitivity utilizing tilted fiber Bragg gratings," *Appl. Opt.*, vol. 46, no. 22, pp. 5456–5460, Aug. 2007.